Electromagnetic modeling of a periodic array of fibers embedded in a panel with multiple fibers missing

Zicheng Liu, Changyou Li, Dominique Lesselier, Yu Zhong

Electromagnetic Modeling of a Periodic Array of Fibers Embedded in a Panel with Multiple Fibers Missing

Zicheng LIU[a,1], Changyou LI[b,2],
Dominique LESSELIER[a], Yu ZHONG[c]

a Laboratoire des Signaux et Syst`emes - UMR8506 CNRS-CentraleSup´elec-U. Paris Sud 3 rue Joliot-Curie, 91192 Gif-sur-Yvette, France
b Singapore University of Technology and Design (SUTD), 8 Somapah Road, Singapore 487372
c A*STAR, Institute of High Performance Computing, Singapore 138632, Singapore

Abstract. Our goal is to detect defects in composite materials composed by multi-layer planar plates with a periodic set of circular cylindrical fibers embedded within each layer. As a starter, the work presented is electromagnetic (EM) modeling and imaging of missing fibers in a fiber array standing in air. The multiple scattering method is utilized to analyze the electromagnetic behavior, and the corresponding imaging model is established directly from Lippman-Schwinger integral formula-tion. With the imaging model, standard MUltiple SIgnal Classification (MUSIC), and the proposed joint sparsity which borrows the idea from sparsity theory, are applied to retrieve the locations of missing fibers. Various numerical results are provided to illustrate availability and accuracy of the modeling and imaging.

Keywords. Electromagnetic modeling, nondestructive testing, periodic fiber array, multipole scattering, MUSIC, joint sparsity

Introduction

Fiber-based laminated composite materials are widely used in aeronautic and automotive industries due to their advantageous characters in terms of stiffness and strength. In the applications, a challenge for safety consideration is to detect and at least locate poten-tial defects in the fiber-based materials using electromagnetic sources and probes. As an example, there may be missing or misplaced fibers, or voids or other damages produced during manufacturing and/or in-service. Experimentations are not referred here. However, carbon-fiber composites are tested with radio frequency eddy current technology in [1] and glass-fiber ones with reflective terahertz time domain spectroscopy [2], which paved the way to the concerned case.

Two main steps follow: one needs an accurate enough scattering model (forward problem) and a high-resolution imaging solution (inverse problem). Here, one is concerned with the time-harmonic electromagnetic response of fiber-reinforced composite

[1]Corresponding Author. E-mail: zicheng.liu@l2s.centralesupelec.fr.
[2]The work has been performed when the second author was in L2S.

laminates as stacks of planar layers [3] (laminates), and high-resolution imaging approaches to get the positions of defects inside.

As a preliminary to the above, emphasis is put onto a structure made of a finite set of circular cylindrical fibers in air. All fibers are identical, orientated the same way and periodically arranged with their centers aligned and at same distance from one another except multiple missing fibers, which actually disorganizes the whole structure.

Both the response to a given excitation (plane wave or line source) and the specific Green's function of the original, intact structure (thereafter assumed to be disorganized) can be handled by means of the multiple scattering method [4], letting the fields inside and outside the fibers being properly multipole expanded. The background field is perturbed by the fact that fibers have been removed and their scattering contribution can be evaluated via a Lippman-Schwinger integral formulation [4]. The integral in explicit form leads to the imaging model which establishes a link between background field and locations of missing fibers.

Since defects as missing fibers are the only ones in consideration, all that one needs is to retrieve their indices (or labels) within the array (which associates with their locations). To do so, the classical MUltiple SIgnal Classification (MUSIC) imaging method [5] is implemented to test the EM modeling and the defects localization. Then, to enhance the discrimination ability, since rare defects exist in the defectuous material, a sparsity-tailored reconstruction method, called joint sparsity, is put forth. Borrowing ideas from pioneering works about Directions of Arrival (DOA) searches [6], the proposed method utilizes the fact that sparsity is invariant when different illuminations are considered.

1. Electromagnetic behavior analysis

1.1. Description of configuration

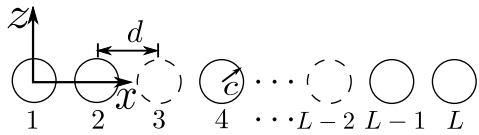

Figure 1. The fiber array in free space, circles with dashed contour indicating missing fibers

The structure which one deals with is sketched in Figure1. Circular cylindrical fibers all orientated into the same direction y with same transverse cross-section within the x,z plane and same radius c are considered. The said cross-sections have their centers equally spaced with distance d in the x direction (periodicity of the array, when sound, see next). The material of each fiber is linear isotropic with relative permittivities ε_l and is (for simplicity at this stage) non magnetic $\mu_l = 1$, $l = 1,2,\ldots,L$, L being the overall number of fibers. In this fiber array, defects seen as missing fibers are characterized by $\varepsilon_l = 1$, and actual ones are with $\varepsilon_l = \varepsilon_r$. The incident field is a TM (or E-polarized) wave.

1.2. Multiple scattering method

The electromagnetic response when a plane wave or a line source is taken as the source of the incident wavefield impinging upon the fiber array is analyzed with the multiple scattering method. Key to this approach is the field representation via a multipole expansion. Specifically, the field in the vicinity of the l-th fiber is expressed as

$$E_y(\mathbf{r}) = \sum_{m=-\infty}^{\infty} \left[A_m^l J_m(kr_l) + B_m^l H_m^{(1)}(kr_l) \right] e^{im\theta_l}, \tag{1}$$

wherein i is the imaginary unit, k is the wavenumber in air, $\mathbf{r} = (r_l, \theta_l)$ are the polar coordinates of the observation point in the local coordinate system with origin at the center of l-th fiber, J_m and $H_m^{(1)}$ are the first-kind Bessel and Hankel functions of order m, A_m^l and B_m^l are the coefficients of the background incoming wave and outgoing wave associated with the l-th fiber. Since the wave incoming upon the l-th fiber is composed by fields scattered by all other fibers, as well as the actual incident field generated by the emitting sources, the coefficients relate as

$$A_m^l = \sum_{j=1, j\neq l}^{L} \sum_{n=-\infty}^{\infty} S_{m-n}^{l-j} B_n^j + K_m^l. \tag{2}$$

In the above $S_{m-n}^{l-j} = H_{m-n}^{(1)}(k|l-j|d)\, e^{i(m-n)\arg(l-j)}$ are translation terms, and K_m^l are the coefficients of actual incident field with, for a line source, $H_m^{(1)}\left(kr_l^s\right) e^{-im\theta_l^s}/4i$ and, for a plane wave, $E_{inc}(-1)^m e^{i(k\cos\theta_{inc} ld - im\theta_{inc})}$; in the latter expressions $\left(r_l^s, \theta_l^s\right)$ are coordinates of the line source in the local polar coordinate system, E_{inc} and θ_{inc} are the amplitude and incident angle of the plane wave. The short form of Eq. (2) is $\mathbf{A} = \mathbf{SB} + \mathbf{K}$, within which column vectors $\mathbf{A} = [A_m^l]$, $\mathbf{B} = [B_m^l]$, $\mathbf{K} = [K_m^l]$, and matrix $\mathbf{S} = [S_{m-n}^{l-j}]$.

Another linear relation between $\mathbf{A}$ and $\mathbf{B}$ can be derived from the boundary conditions at the fibers with field expansion inside the l-th fiber as

$$E_y(\mathbf{r}) = \sum_{m=-\infty}^{\infty} \left[C_m^l J_m(k_l r_l) + Q_m^l H_m^{(1)}(k_l r_l) \right] e^{im\theta_l}, \tag{3}$$

where $k_l = k\sqrt{\varepsilon_l}$ and $Q_m^l = \chi_l J_m(k_l r_l^s) e^{-im\theta_l^s}/4i$ are coefficients of the field scattered by an interior line source located at $\left(r_l^s, \theta_l^s\right)$. The term χ_l equals to 1 when the line source is present and 0 otherwise. Matching tangential components of electric field and magnetic field across fiber boundaries, coefficients in the above can be conveniently linked together in terms of reflection matrices $\mathbf{R}$ and $\mathbf{R}'$, and transmission matrices $\mathbf{T}$ and $\mathbf{T}'$ by equations $\mathbf{B} = \mathbf{RA} + \mathbf{TQ}, \mathbf{C} = \mathbf{T}'\mathbf{A} + \mathbf{R}'\mathbf{Q}$, where $\mathbf{C} = \left[C_m^l\right]$ and $\mathbf{Q} = \left[Q_m^l\right]$. Together with Eq. (2), a system of linear equations in $\mathbf{A}$, $\mathbf{B}$, and $\mathbf{C}$ is built and solutions can be easily derived from

$$\mathbf{B} = (\mathbf{I} - \mathbf{RS})^{-1} (\mathbf{RK} + \mathbf{TQ}), \tag{4}$$

which plays a key role in the calculation of $\mathbf{B}$ and $\mathbf{C}$, and consequently the field in the whole space follows.

1.3. Imaging model for detecting defects

To link the background field and locations of missing fibers, the imaging model needs to be established. In effect, the possibility of finding missing fibers in the fiber array by analyzing its electromagnetic response comes from the disturbance of the background field due to these defects. Its evaluation is carried out with the help of the Lippman-Schwinger integral formulation

$$\widetilde{E}_y(\mathbf{r}) - E_y(\mathbf{r}) = \sum_{l=1}^{L} \int_{D_l} \mathbf{G}(\mathbf{r},\mathbf{r}') \left(k_l^2 - k^2\varepsilon_r\right) \widetilde{E}_y(\mathbf{r}')\, \mathrm{d}\mathbf{r}', \tag{5}$$

where E_y denotes the total field in the well-organized structure herein and parameters with '$\sim$' above are associated with the subsequently disorganized structure, D_l is the surface area of the l-th missing fiber, and $\mathbf{G}(\mathbf{r},\mathbf{r}')$ is the Green's function when the line source is located at $\mathbf{r}'$ and the fiber array is well-organized. Substituting the expression of $\mathbf{G}(\mathbf{r},\mathbf{r}')$ obtained by letting $\mathbf{K} = \mathbf{0}$ and $\chi_l = 1$, and that of $\widetilde{E}_y$ by letting $\mathbf{Q} = \mathbf{0}$ and $k_l = k$ into Eq. (5), the involved integral can be reduced into a simpler form

$$\widetilde{E}_y(\mathbf{r}) - E_y(\mathbf{r}) = \sum_{l=1}^{L} \sum_{m=-\infty}^{\infty} b_m^l H_m^{(1)}(kr_l) e^{im\theta_l}, \tag{6}$$

which is a summation of scattered fields by the entire set of fibers with coefficients b_m^l, and b_m^l calculated as

$$\mathbf{b} = (\mathbf{I} - \mathbf{RS})^{-1}\mathbf{Tq}, \tag{7}$$

where $\mathbf{b} = \left[b_m^l\right]$, $\mathbf{q} = \left[q_m^l\right]$, and $q_m^l = (\sqrt{\varepsilon_r}J_{m+1}(k\sqrt{\varepsilon_r}c)J_m(kc) - J_m(k\sqrt{\varepsilon_r}c)J_{m+1}(kc)) \cdot ikc\pi\chi_l\widetilde{C}_m^l/2$.

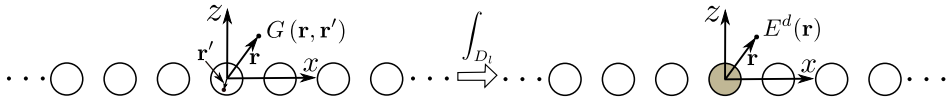

Figure 2. Sketch for physical interpretation of Lippman-Schwinger integral formulation.

The Lippman-Schwinger integral formulation Eq. (5), together with Eqs. (6) and (7), can be physically interpreted by Figure 2, where the dot in the left part stands for a line source located at $\mathbf{r}'$, the gray fiber in the right part is the cylindrical source having same cross-section as the removed fiber and $E_y^d(\mathbf{r}) = \widetilde{E}_y(\mathbf{r}) - E_y(\mathbf{r})$ is the background field due to this cylindrical source. The coefficients of the field scattered by the cylindrical source within the l-th fiber are q_m^l, and the field scattered by each fiber, in the background medium, is with coefficients b_m^l. Denoting $\mathbf{H} = [H_m^{(1)}(kr_l)e^{im\theta_l}]$, $E_y^d(\mathbf{r})$ can be written as

$$E_y^d(\mathbf{r}) = \mathbf{H}(\mathbf{I} - \mathbf{RS})^{-1}\mathbf{Tq}. \tag{8}$$

Be a receiver array with N_r elements and sources array with N_s elements utilized for the testing. For the ν-th source, values of $E_y^d(\mathbf{r})$ collected by the receiver array can

compose a column vector $\mathbf{g}_\nu$ with dimension N_r, $\nu = 1,2,\ldots,N_s$. The data matrix $\mathbf{Y}$, or Muti-Static Response (MSR) [5], can be constructed by taking them as columns, *i.e.* $\mathbf{Y} = [\mathbf{g}_1, \mathbf{g}_2, \ldots, \mathbf{g}_{N_s}]$. Since, the expression $\mathbf{H}(\mathbf{I} - \mathbf{RS})^{-1}\mathbf{T}$ is invariant with the sources, an initial imaging model can be derived as an extension of Eq. (8),

$$\mathbf{Y} = \mathbf{H}(\mathbf{I} - \mathbf{RS})^{-1}\mathbf{TF}, \tag{9}$$

where $\mathbf{F} = [\mathbf{q}_1, \mathbf{q}_2, \ldots, \mathbf{q}_{N_s}]$.

1.4. Zero-mode approximation

The number of modes cannot be infinite in multipole expansions. As a conclusion in [4], $\sum_{m=-\infty}^{\infty}$ is truncated to $\sum_{m=-M}^{M}$ with $M = \text{int}\left((k\sqrt{\varepsilon_r}c)^{1/3} + k\sqrt{\varepsilon_r}c + 5\right)$, in which int is the operator yielding the integer part. With a low-frequency incident field, $(k\sqrt{\varepsilon_r}c)^{1/3} + k\sqrt{\varepsilon_r}c$ can be smaller than 1, then M is reduced to 0 without the security factor 5. With this point, an approximated imaging model can be obtained by letting $M = 0$, *i.e.*,

$$\mathbf{Y} = \left(\mathbf{H}(\mathbf{I} - \mathbf{RS})^{-1}\mathbf{T}\right)^0 \mathbf{F}^0 + \mathbf{N}^0, \tag{10}$$

where the superscript 0 identifies matrices that are only including the zero-th mode, and $\mathbf{N}^0$ is the resulting approximation error.

Benefiting from this approximation, the dimensions of the matrices involved are largely reduced, which lightens the burden of the following reconstruction procedures. Taking into account additive noise $\mathbf{N}_a$ in the collected data, and setting $\mathbf{Z} = \left(\mathbf{H}(\mathbf{I} - \mathbf{RS})^{-1}\mathbf{T}\right)^0$, $\mathbf{S} = \mathbf{F}^0$ and $\mathbf{N} = \mathbf{N}^0 + \mathbf{N}_a$ for convenience, one gets the imaging model in the noisy case as

$$\mathbf{Y} = \mathbf{ZS} + \mathbf{N}. \tag{11}$$

From the definition of $\mathbf{S}$, one can find the correspondence between the indices of missing fibers and the positions of non-zero rows in $\mathbf{S}$. Specifically, the l-th row of $\mathbf{S}$ will be non-zero when the l-th is missing, and null otherwise.

2. Reconstruction methods

Standard MUSIC and the proposed joint sparsity method are adopted to solve for $\mathbf{S}$ in Eq. (11). Literature about MUSIC is abundant, so only joint sparsity is commented.

2.1. MUSIC

The singular value decomposition of the matrix $\mathbf{S}$ reads as

$$\mathbf{Y} = \mathbf{UDV}^*, \tag{12}$$

where $*$ denotes the conjugate transpose, and $\mathbf{D}$ is a diagonal matrix composed from the singular values. According to the distribution of singular values [7], $\mathbf{U}$ can be divided into signal space $\mathbf{U}_s$ and noise space $\mathbf{U}_n$. The estimation function is defined as

$$\hat{s}^l = \frac{\mathbf{Z}_l \mathbf{Z}_l^*}{\mathbf{Z}_l^* \mathbf{U}_n \mathbf{U}_n^* \mathbf{Z}_l}, \tag{13}$$

where $\mathbf{Z}_l$ indicates the l-th column of $\mathbf{Z}$. Since the denominator goes to zero when the l-th fiber is missing, defects are shown as peaks in the curve of vector $\hat{\mathbf{s}} = [\hat{s}^l]$.

2.2. Joint sparsity

In general applications, only few fibers are faulty (missing). As exhibited from the composition of $\mathbf{S}$, each column has few non-zero elements, *i.e.*, each column of $\mathbf{S}$ is sparse. Furthermore, since the indices of missing fibers are invariant with the emitting sources, different columns of $\mathbf{S}$ share joint positions of non-zero elements, *i.e.*, different columns enjoy joint sparsity.

To take advantage of this prior knowledge, a specific regularization is set forth. Letting s^l as the l_2-norm of the l-th row of $\mathbf{S}$, results from different rows can compose a vector $\mathbf{s} = [s^1, s^2, \ldots, s^N]$. In this way, the knowledge about joint sparsity is converted into the sparsity in $\mathbf{s}$ while the information desired is saved simultaneously. Since sparsity can be accurately evaluated via the l_0 norm which counts the number of non-zero elements, the following optimization yields $\mathbf{s}$:

$$\min \ ||\mathbf{s}||_0, \text{ subject to } ||\mathbf{Y} - \mathbf{Z}\mathbf{S}||_F^2 \leq \tau^2 \text{ and } s^n = ||\mathbf{S}^n||_2, l = 1, 2, \ldots, L, \tag{14}$$

where $||\mathbf{s}||_0$ stands for the l_0-norm of $\mathbf{s}$, s^l is the l_2-norm of the l-th row of $\mathbf{S}$, and τ is the parameter constraining the energy of residual. However, solving $\mathbf{s}$ in Eq. (14) is qualified as a NP-hard problem, requiring an exhaustive enumeration of all $\binom{L}{P}$ possible locations of nonzero entries in $\mathbf{s}$. Fortunately, optimization based on l_1-norm

$$\min \ ||\mathbf{s}||_1, \text{ subject to } ||\mathbf{Y} - \mathbf{Z}\mathbf{S}||_2^2 \leq \tau^2 \text{ and } s^n = ||\mathbf{S}^n||_2, l = 1, 2, \ldots, L \tag{15}$$

can also exactly recover $\mathbf{s}$ when sufficient collected data are available. This problem here is converted into the second order cone programming (SOCP) form [8] and solved by a standard free package SeDuMi [9].

As a further step, to reduce the effect of noise, the data matrix $\mathbf{Y}$ can be pre-processed by mapping $\mathbf{Y}$ onto its signal subspace, *i.e.*,

$$\mathbf{Y}_v = \mathbf{Z}\mathbf{S}_v + \mathbf{N}_v, \tag{16}$$

where $\mathbf{Y}_v = \mathbf{Y}\mathbf{V}_s$, $\mathbf{S}_v = \mathbf{S}\mathbf{V}_s$, $\mathbf{N}_v = \mathbf{N}\mathbf{V}_s$, and $\mathbf{V}_s$ is the signal subspace of $\mathbf{V}$. The choice of $\mathbf{V}_s$ obeys the same criterion as the one of $\mathbf{U}_s$ in MUSIC. Since $\mathbf{N}$ and $\mathbf{V}_s$ are uncorrelated with each other, the noise effect on the retrieval results can be reduced. And, since $\mathbf{S}$ is multiplied by $\mathbf{V}_s$ on the right side, the information about the index of missing fibers is saved in $\mathbf{S}_v$. Thus $\mathbf{S}_v$ can be reconstructed in the same way as described in Eq. (15).

3. Numerical results

First, the accuracy of the multiple scattering method is validated by comparing it with the finite-element software COMSOL, then standard MUSIC and joint sparsity method are

applied to locate missing fibers. The proposed example is a periodic array of 65 circular cylindrical fibers standing in air. Material in each is either carbon ($\varepsilon_r = 12$, conductivity $\sigma = 3 \times 10^2$ S/m) or glass ($\varepsilon_r = 6$). Indices run from -32 to 32. Distance between centers of adjacent fibers is $d = 0.01$mm, and radius $c = 0.2d$. Validation of the electromagnetic

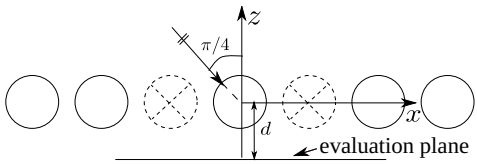

Figure 3. Validation by COMSOL with (-1)-th and 1-th carbon fibers missing, incident wavelength $\lambda^{inc} = d$.

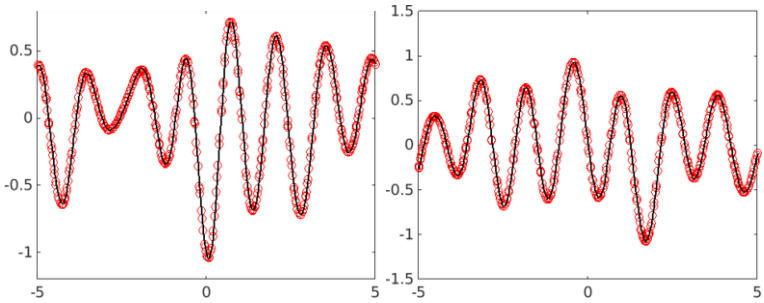

Figure 4. Validation of (a) imaginary part and (b) real part of the electric field with the disorganized structure.

modeling is conducted by letting a plane wave impinge on a disorganized carbon-fiber array with incident angle $\pi/4$. In this array, fibers with indices -1 and 1 are missing. The incident wave is with wavelength $\lambda^{inc} = d$. Data for comparisons are collected from the total field on the evaluation line, as shown in Figure 3, ranging from $-5d$ to $5d$ in the x direction. To validate both amplitude and phase, real and imaginary parts are compared. Refer to Figure 4. The circles represent the results with the multiple scattering method, results of COMSOL are denoted by the solid line. It can be seen that the results exhibited are in excellent agreement.

Then, imaging results are displayed according to Figure 5. The z axis is taken as the central line, 100 line sources and 100 receivers are uniformly placed along the lines $z = d$ and $z = -d$, respectively. The interval between adjacent sources or receivers is $d/2$. Additive Gaussian noise is accounted for signal to noise ratio (SNR) of 20 dB.

Figure 6 shows the detection results with both standard MUSIC and the joint sparsity method, the vertical dashed lines indicating the true indices of missing fibers. It can be observed that, no matter whether the fiber be mostly conductive (carbon) or dielectric (glass), both methods yield accurate estimates of the locations of the missing fibers.

4. Conclusions

Investigations about a fiber array with missing fibers have been performed. To model the fields, the multiple scattering method has been utilized and independently validated.

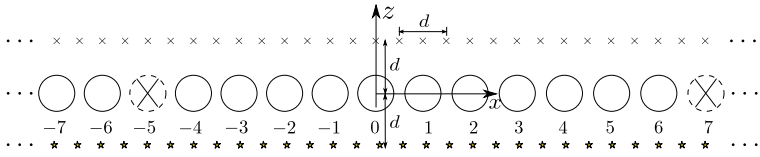

Figure 5. Configuration of imaging

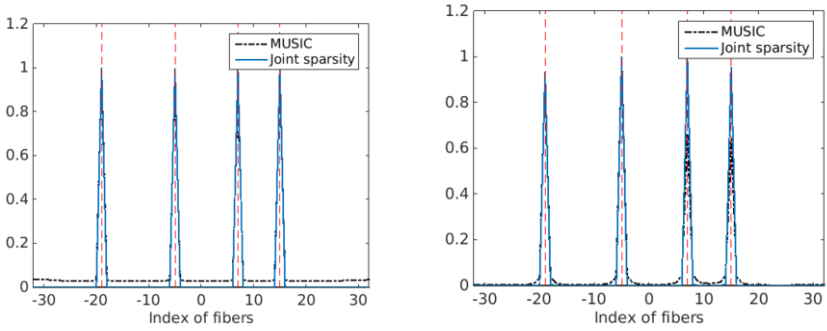

(a) (b)

Figure 6. Imaging results of missing (a) carbon (b) glass fibers, with indices [-19, -5, 7, 15], $N_r = N_s = 100$, $f = 60$GHz, $d = 0.1$mm, $c = 0.2d$, SNR = 20 dB

Imaging is directly derived from Lippman-Schwinger integral formulation, and then is simplified with the zero-mode approximation. Both standard MUSIC and joint sparsity methods have been applied to retrieve the indices of missing fibers. However, at high frequency, the zero-mode approximation error cannot be neglected, which might call for establishment of a new imaging model to make use of more modes. Investigations on the single-layer structure (involving a matrix material different from air) are also foreseen.

References

[1] H. Heuer, et al., Review on quality assurance along the CFRP value chain Non-destructive testing of fabrics, preforms and CFRP by HF radio wave techniques, *Composites Part B*, **77** (2015), 494-501.

[2] C. Stoik, M. Bohn, and J. Blackshire, Nondestructive evaluation of aircraft composites using reflective terahertz time domain spectroscopy, *NDT&E Int.*, **43** (2010), 106-115.

[3] C.Y. Li, D. Lesselier, and Y. Zhong, Full-wave model and numerical study of electromagnetic plane wave scattering by multilayered, fiberbased periodic composites, *Radio Science*, **50** (2015), 688-697.

[4] J-P. Groby and D. Lesselier, Localization and characterization of simple defects in finite-sized photonic crystals, *J. Optical Soc. Amer. A*, **25** (2008), 146-152.

[5] E. Iakovleva, S. Gdoura, D. Lesselier, and G. Perrusson, Multistatic response matrix of a 3-D inclusion in half space and MUSIC imaging, *IEEE Trans. Antennas Propagat.*, **55** (2007), 2598-2609.

[6] D. Malioutov, M. Çetin, and A. S. Willsky, A sparse signal reconstruction perspective for source localization with sensor arrays, *IEEE Trans. Signal Process.*, **53** (2005), 3010-3022.

[7] P. C. Hansen, T. K. Jensen, and G. Rodriguez, An adaptive pruning algorithm for the discrete l-curve criterion, *J. Computation. Applied Math.*, **198** (2007), 483-492.

[8] S. Boyd and L. Vandenberghe, Convex optimization, *Cambridge Univ. Press*, Cambridge, 2004.

[9] J. F. Sturm, Using SeDuMi 1.02, a MATLAB toolbox for optimization over symmetric cones, *Optim. Methods Softw.*, **11** (2003), 625-653.